Mon. Not. R. Astron. Soc. **000**, 1–10 (1997) Printed 29 August 1997 (MN LaTeX style file v1.3)

Spectroscopy of the roAp star α Cir. I. Velocities of Hα and metal lines.

I. K. Baldry[1], T. R. Bedding[1], M. Viskum[2], H. Kjeldsen[2,3], S. Frandsen[2]

[1] *Chatterton Astronomy Department, School of Physics, University of Sydney, NSW 2006, Australia*
[2] *Institute of Physics and Astronomy, University of Aarhus, DK-8000 Aarhus C, Denmark*
[3] *Theoretical Astrophysics Center, University of Aarhus, DK-8000 Aarhus C, Denmark*

Re-submitted 1997 September. Received in original form 1997 July. Ref. MX601.

ABSTRACT

We present radial velocity measurements of the rapidly oscillating Ap (roAp) star, α Cir, obtained from dual-site observations with medium-dispersion spectrographs. The amplitude and phase of the principal pulsation mode vary significantly, depending on which line is being measured. The amplitude is observed to be as high as $1000\,\mathrm{ms}^{-1}$ in some wavelength bands, despite a previous upper limit of $36\,\mathrm{ms}^{-1}$. Furthermore, some lines are apparently pulsating in anti-phase with others. We suggest this indicates a high-overtone standing wave with a velocity node in the atmosphere of the star.

Key words:
stars: individual: α Cir — stars: oscillations — techniques: radial velocities — stars: chemically peculiar.

1 INTRODUCTION

Rapidly oscillating Ap (roAp) stars are a sub-class of the chemically peculiar magnetic (Ap or CP2) stars. The Ap phenomenon is characterised by spectra with anomalously strong lines of Si, Sr, Cr, other iron peak elements, Eu and other rare earth elements. The stars also have strong global magnetic fields of typically a few kG. The cause of the abundance anomalies is thought to be magnetically guided chemical diffusion, made possible because Ap stars have slower rotation rates than normal A stars. Some Ap stars also show evidence of an inhomogeneous distribution of elements (in spots) on the surface of the star (Rice & Wehlau 1991). Despite the name, the Ap stars range in temperature from spectral type B8 to F0 (luminosity class IV-V). At the cool-end of the range, the Ap stars overlap the instability strip and this is where the roAp stars are found. However, not all the Ap stars in the instability strip have been observed to pulsate (Mathys, Kharchenko & Hubrig 1996). A review of roAp stars with a comprehensive list of references is given by Kurtz (1990). Later reviews are given by Matthews (1991, 1997) and Martinez & Kurtz (1995a, 1995b), and a review on the theoretical aspects is given by Shibahashi (1991).

1.1 α Cir

α Circini (HR 5463, HD 128898, V=3.2, spectral type Ap SrEu(Cr)) is the brightest of the known roAp stars. It is situated at a distance of 16.4±0.2 pc (parallax 61.0±0.6 mas, HIP 71908, Perryman et al. 1997) and is a visual binary (secondary, V=8.2) with a separation of 15.6 arcsec. Kurtz & Martinez (1993) determined an equivalent spectral type of A6V ($T_{\rm eff}$ = 8000 K), while Kupka et al. (1996) have derived $T_{\rm eff} = 7900 \pm 200$ K and $\log g = 4.2 \pm 0.15$.

Previous observations of this star in photometry (Kurtz et al. 1994) have shown that its principal pulsation mode is a pure oblique dipole mode (ℓ=1) with a frequency of 2442 μHz (P = 6.825 min). Kurtz et al. (1994) measured the amplitude of the principal mode to be 2.55 mmag (Strömgren v). They also found two rotationally split sidelobes (∼0.27 mmag), four weaker modes (∼0.15 mmag) and the first harmonic of the principal mode (∼ 0.20 mmag). It has also been observed that the photometric amplitude depends on the wavelength (Weiss et al. 1991, Medupe & Kurtz 1997), with amplitude decreasing with increasing wavelength. In Section 5.3 we relate these wavelength dependent photometric amplitudes to our results.

The vast majority of studies of roAp stars have been made using photometry. In three stars, HR 1217 (Matthews et al. 1988), γ Equ (HR 8097; Librecht 1988, Kanaan & Hatzes 1997) and 10 Aql (HR 7167; Matthews & Chagnon 1997), have oscillations been convincingly detected in Doppler shift. For α Cir, based on the photometric amplitude given above, the relation of Kjeldsen & Bedding (1995) predicts a velocity amplitude of $160\,\mathrm{ms}^{-1}$. Belmonte et al. (1989) claimed a detection in α Cir at an amplitude of $1000\,\mathrm{ms}^{-1}$ using a line at 5317.4Å, but this result was in doubt given that Schneider & Weiss (1989) had set an upper

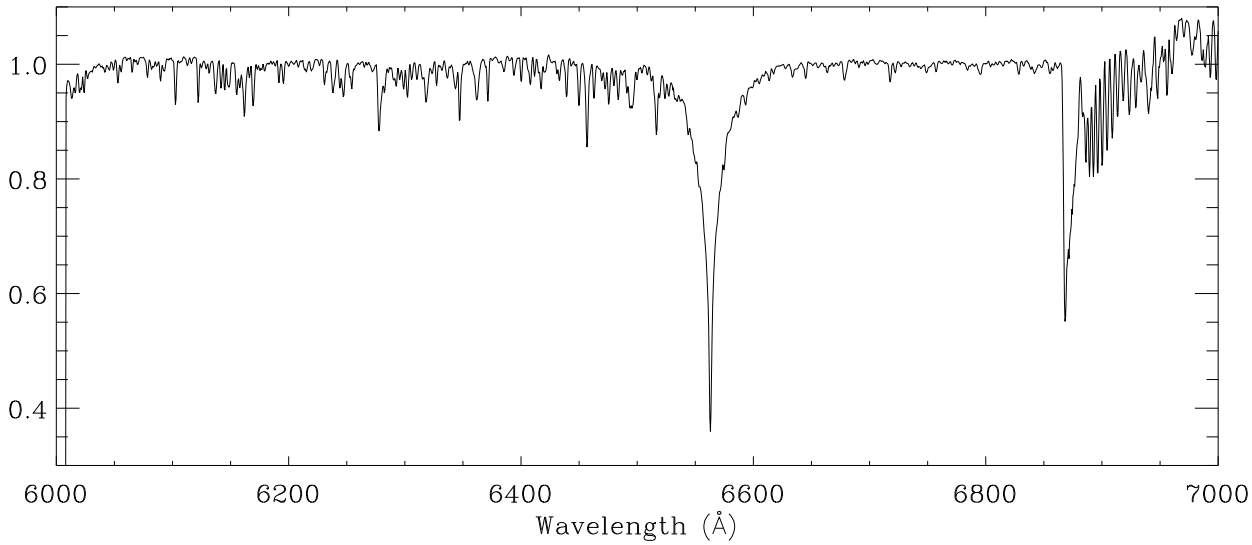

Figure 1. Template spectrum from the Stromlo data set.

limit of 100 ms^{-1} for possible radial velocity variations, using a wavelength region from 6450Å to 6500Å. More recently, an upper limit for α Cir of only 36 ms^{-1} (peak-to-peak) was set by Hatzes & Kürster (1994) at the frequency of the principal photometric pulsation mode, using a wavelength region from 5365Å to 5410Å. In this paper we examine the radial velocity amplitude of the principal mode for different wavelength bands. From our work (see also Viskum et al. 1997) and from the work by Kanaan & Hatzes (1997) on γ Equ, it is apparent that the velocity amplitude in roAp stars can vary significantly from line to line, and that previous upper limits reflect averages over the wavelength regions used.

2 OBSERVATIONS

We have obtained intermediate-resolution spectra of α Cir using the coudé spectrograph (B grating) on the 74 inch (1.88m) Telescope at Mt. Stromlo, Australia and the DFOSC spectrograph mounted on the Danish 1.54m at La Silla, Chile. We have a total of 6366 spectra from a period of 2 weeks in 1996 May (Table 1).

The Stromlo data consist of single-order spectra, projected onto a 2K Tektronix CCD, with a wavelength coverage of 6000Å to 7000Å. The dispersion was 0.49Å/pixel and was nearly constant across the spectrum, with a resolution of approx. 1.5Å set by the slit width of 2 arcsec. The typical exposure time was 28 seconds, with an over-head between exposures of 17 seconds. The average number of photons/Å in each spectrum was about 800 000.

The La Silla data consist of echelle spectra containing six orders, projected onto a 2K LORAL CCD, with a total wavelength coverage of 4500Å to 8000Å. For this paper, we have only considered the order containing Hα, which covers the range 6200Å to 7200Å. The dispersion varied from 0.51Å/pixel to 0.70Å/pixel across this order, giving a similar resolution to the Stromlo data. For the La Silla data, the typical exposure time was 40 seconds with an over-head of 42 seconds. The average number of photons/Å in the Hα order of each spectrum ranged from about 480 000 at the blaze peak (6700Å) to about 120 000 at the blue end (6200Å).

Table 1. Log of the observations of α Cir.

UT-date	Site	No. of hours	No. of spectra	Julian dates −2450000
1996 May 05	Stromlo	0.97	23	209.31 – 209.35
1996 May 06	Stromlo	3.66	249	210.19 – 210.34
1996 May 09	La Silla	4.13	123	212.77 – 212.94
1996 May 09	Stromlo	12.05	785	212.84 – 213.35
1996 May 10	La Silla	3.78	142	213.77 – 213.92
1996 May 10	Stromlo	11.82	640	213.83 – 214.32
1996 May 11	La Silla	4.15	151	214.76 – 214.93
1996 May 11	Stromlo	9.17	735	214.82 – 215.21
1996 May 12	La Silla	3.98	156	215.77 – 215.93
1996 May 12	Stromlo	8.19	447	216.01 – 216.35
1996 May 13	La Silla	4.35	186	216.76 – 216.94
1996 May 13	Stromlo	12.72	856	216.82 – 217.35
1996 May 14	La Silla	2.09	88	217.76 – 217.84
1996 May 14	Stromlo	12.52	862	217.83 – 218.35
1996 May 15	La Silla	4.58	156	218.75 – 218.94
1996 May 15	Stromlo	6.33	303	219.09 – 219.35
1996 May 17	La Silla	4.08	121	220.76 – 220.93
1996 May 18	La Silla	4.16	159	221.76 – 221.93
1996 May 19	La Silla	3.82	184	222.74 – 222.90

3 REDUCTIONS

3.1 Extraction of Spectra

IRAF procedures were used to reduce the data from 2D images to 1D spectra. These involved bias subtraction, flat-field division, and extraction of the orders including background scattered-light subtraction. Additionally the Stromlo data were corrected for non-linearities on the CCD image after

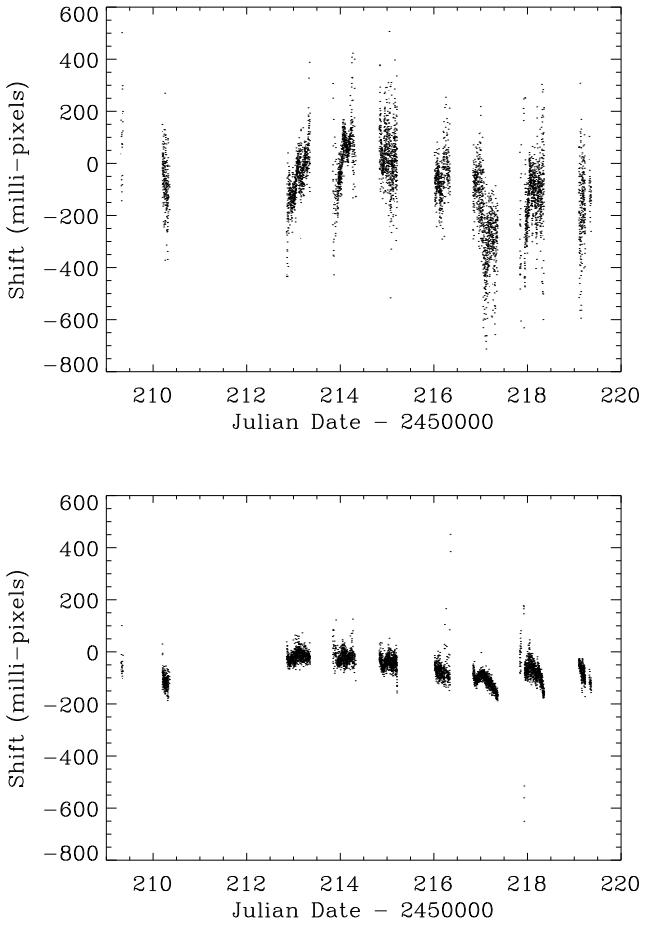

Figure 2. Shifts of the Hα line (band no. 88), from the Stromlo data set. **Upper**: using no reference. **Lower**: using a telluric band (no. 80) as a reference.

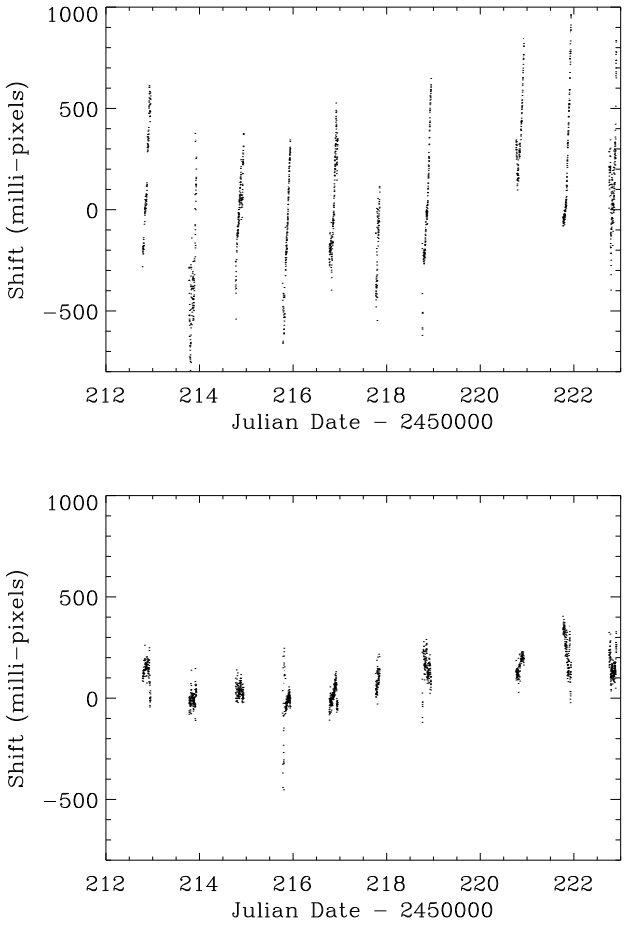

Figure 3. Shifts of the Hα line (band no. 88), from the La Silla data set. **Upper**: using no reference. **Lower**: using a telluric band (no. 80) as a reference.

bias subtraction (Section 4 from Gilliland et al. 1993). This was necessary because the ratio between expected-counts and measured-counts varied by 7% from low-light levels to digital saturation. After correction, the data were linear to within 1%. The La Silla data were measured to be linear within 0.5%.

After reduction to the 1D stage, the spectra were fitted using the IRAF procedure, continuum, in which low points are excluded until a fit is obtained close to the continuum level. A third order polynomial fit was used for the Stromlo data and a second order fit for the La Silla data. For each data set, a template spectrum was obtained by averaging 25 high-quality spectra (Figure 1).

3.2 Cross-correlations

The spectra obtained from Mt. Stromlo were divided into 89 unequal wavelength bands (Table 3). Except for the region containing Hα, the bands were non-overlapping and typically contained a few lines. The boundaries were chosen at places where two or three pixels were nearly at the same level (close to the continuum). In the case of Hα, we defined four bands of different widths, each centred on the core (band nos 85–88). Only 66 of these bands were used from the La Silla spectra because of the different wavelength coverage.

A cross-correlation technique was applied to measure the Doppler shift of each band in each spectrum, relative to the same band in the template spectrum. The following procedure was applied:

(i) a linear local continuum fit was applied across the band using the edge pixels;

(ii) the spectral band was linearly rebinned by a factor of 40 and 1.0 was subtracted such that the edge pixels were nearly zero;

(iii) a half-cosine filter was applied across 3 pixels at the edges so that there was a smooth transition between zero outside the band and nearly zero on the edge pixels;

(iv) the spectral band was cross-correlated (using FFTs) with the band from the template spectrum, which had been processed in the same way;

(v) the peak of the cross-correlation function was found by fitting a quadratic to 9 points around the peak point.

With this procedure, we could measure shifts to within 0.02 pixels (400 ms^{-1}) in most of the spectra.

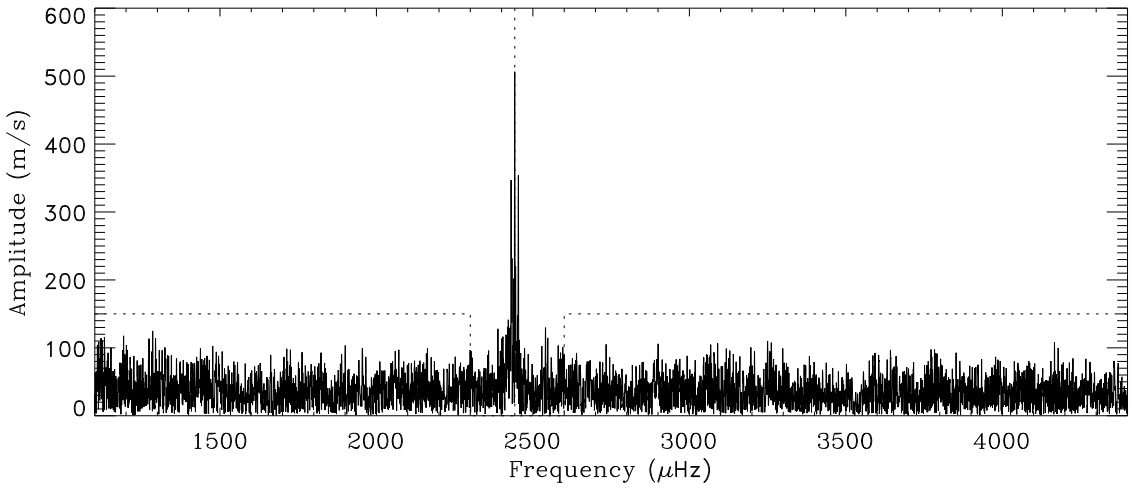

Figure 4. Amplitude spectrum for wavelength band no. 18, using the Stromlo data set. This figure clearly shows a peak at the principal frequency (2442 μHz), and shows the regions which were used to calculate the noise-level (1100–2300 μHz and 2600–4400 μHz). The side lobes to the main peak are caused by aliasing. The signal-to-noise ratio of the principal peak in this spectrum is 11.5.

3.3 Velocity Reference

The dominant cause of scatter in the velocity measurements is the global shifts of the light on the spectrograph. To correct for this, we have used the strong telluric O_2 absorption band around 6870Å as a velocity reference (band no. 80). The noise factors associated with using a telluric reference are the instability of the telluric atmospheric band and the changes in dispersion of the spectrograph, which affects the relative shift between a target band and the reference band. In our data, the variance of the noise when using the telluric reference was about one-tenth of the variance when using no reference, when measuring a target band about 300Å away from the telluric reference. Note that we were only interested in high-frequencies (periods less than 15 minutes) for this analysis, so that slow drifts of the spectrograph and an absolute measure of the radial velocity of the star were not important.

Figures 2–3 show the Stromlo and La Silla Hα velocity time-series, with the improvement in noise level that is made when a telluric band is used as a velocity reference. This is particularly evident for the Hα Doppler shift, for which the noise is dominated by instrumental factors rather than photon-noise.

3.4 Time-series Analysis

The time-series for the 88 different bands (not including the velocity reference) were high-pass filtered, and then cleaned for bad data points by removing any points lying outside $\pm$6.5 times the median deviation. Next, a weighted least-squares fitting routine was applied to each time series (using heliocentric time) to produce amplitude spectra.

4 RESULTS ON THE PRINCIPAL MODE

We have concentrated on using the Stromlo data for comparison between the different bands. This is because the La Silla data only covers bands 23–88 and also has a higher noise level per spectrum for the cross-correlation measurements. Also, we are only examining the principal pulsation mode with individual bands, therefore there is no need to use the dual-site combined data to reduce aliasing. This allows us to use the La Silla data to check the results obtained using the Stromlo data (Section 4.2).

Table 2. Photometric amplitudes (Johnson B) and frequencies, of the principal mode, measured by Don Kurtz (private comm.). The reference-point (t_0) for the phase measurements is JD 2450215.07527, with the convention that a phase of 0° represents maximum light.

Julian dates −2450000	frequency (μHz)	amplitude (mmag)	phase (degrees)
142 – 272	2442.039±0.002	1.74±0.07	0.0±2.4
213 – 244	2442.022±0.011	1.63±0.12	15.3±7.3

Figure 4 shows the amplitude spectrum of a band with a strong peak at the principal photometric frequency, and Figures 5–6 show that the principal mode is evident even with quite low signal-to-noise ratios (4.4 and 3.1).

We measured the frequency of the principal mode to be 2442.05±0.02 μHz using the Stromlo data set, and 2442.02±0.03 μHz using the combined data from both sites. This is in agreement with photometric frequencies measured in the same time period by Don Kurtz (private comm., see Table 2) as part of an ongoing project of measuring frequency changes in roAp stars (Section 6 from Martinez & Kurtz 1995b, Kurtz et al. 1997). The two calculations from the photometric data, shown in Table 2, are over 130 days and 31 days. We have set our phase reference-point (t_0) to coincide with maximum light, using the first calculation. Our velocity phases are measured at this reference-point, with the convention that a phase of 0° represents maximum velocity (red-shift). For example, a phase of −30° means that the velocity curve lags behind the light curve by 30°. Note

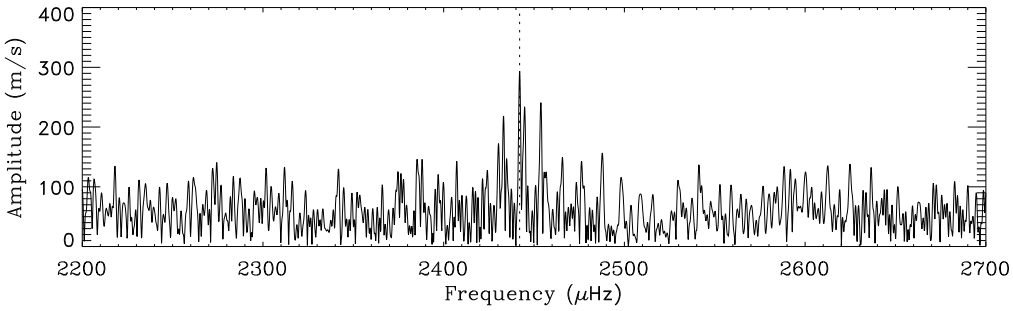

Figure 5. Amplitude spectrum for wavelength band no. 57. The signal-to-noise ratio in this spectrum is 4.4.

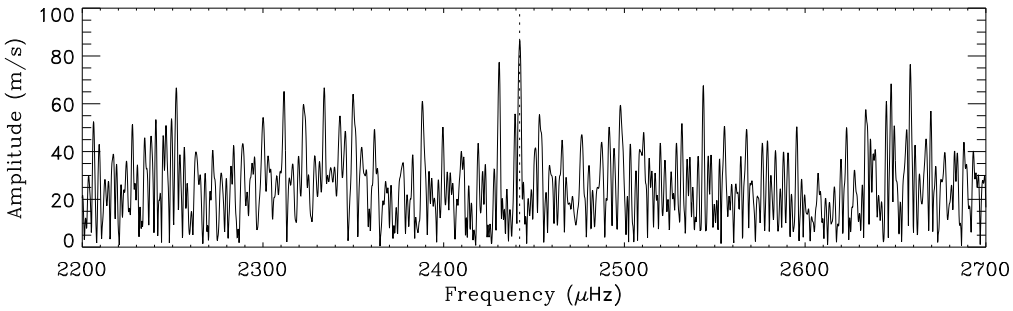

Figure 6. Amplitude spectrum for wavelength band no. 44. The signal-to-noise ratio in this spectrum is 3.1.

that the second calculation indicates that there may have been some frequency changes during the time period of the first. If this is the case, then maximum light may not coincide with the reference-point by up to ∼20° of a cycle.

We have measured the amplitude and phase of each time-series at 2442.03 μHz and estimated the rms-noise level by averaging over surrounding frequencies (1100–2300 μHz and 2600–4400 μHz). See Figure 4 for an example. The results are shown in Table 3.

4.1 Amplitude and Phase Variations

The amplitude and phase of the principal photometric mode vary significantly between different bands, with some bands that are pulsating in anti-phase with others. Figure 7 shows an amplitude vs. phase diagram for bands for which the signal-to-noise ratio in the amplitude spectrum is greater than 3.0. For these bands we can be sure that we have detected the principal pulsation and that the phase is reasonably well defined. For the uncertainty in the amplitude, we have used the rms-noise level directly. For the uncertainty in the phase, we have used simple complex arithmetic to find the maximum change in phase that a rms-noise vector could induce i.e. arcsin (rms-noise/amplitude).

Figure 8 shows a histogram of the phases of the principal mode. Most bands have phases that lie between −60° and 30° but there is also a group of five bands with phases between 180° and 210°. We suggest that these two groups might be associated with two sections of the atmosphere either side of a pulsational node (zero-point). However, there is more variation in the phases than can be accounted for purely by using a standing wave model. Perhaps there is also a travelling component to the pulsational wave in the star's atmosphere. Another possibility is that we are seeing asymmetric temperature (equivalent-width) changes that create apparent Doppler shifts and therefore produce a variety of phases. For example, consider two lines at different wavelengths which are blended. If a temperature change causes the relative strength of the two lines to change then a pseudo-Doppler shift may be measured from the blended profile.

The line identification for the different bands (Table 3) is only an approximate analysis based on synthetic spectra (Friedrich Kupka, private comm.) using recently derived abundances (Kupka et al. 1996). Nearly all the bands that we have measured are composed of blended lines in our spectra. Therefore it has been difficult to determine if there is a pattern associating the line-type with the measured amplitude of the pulsation. One noticeable pattern is that the largest amplitudes occur only in the weaker lines, this is seen from a plot of amplitude vs. total equivalent width of the band (Figure 9). Possibly this is because weaker lines are more likely to be formed in a narrower section of the star's atmosphere and therefore phase smearing between different parts of a pulsation wave is minimised. Kanaan & Hatzes (1997) have also found that the velocity amplitude tends to be higher (up to 1000 ms^{-1}) in the weaker lines of the roAp star γ Equ.

4.2 Comparing the Data Sets

The amplitude vs. phase diagram for the La Silla data is shown in Figure 10. The amplitudes and phases measured from the two data sets are in complete agreement, at the

Table 3. Information on wavelength bands from α Cir showing amplitude and phase at 2442.03μHz from the Stromlo data set. This page of the table shows most of the bands blueward of Hα.

band no.	wavelengths (Å)	total-EW[a] (Å)	amplitude (ms^{-1})	rms-noise[b] (ms^{-1})	signal-to-noise ratio	phase[c] (degrees)	phase-error[d] (degrees)	notes[e] on lines
00	6011.3 – 6018.2	0.143	136	60	2.2	171	26	Mn I
01	6019.1 – 6036.4	0.205	55	49	1.1	51	62	Fe I, Mn I, Si I
02	6037.7 – 6047.1	0.066	227	88	2.6	105	23	S I, Ce II, Fe II
03	6048.5 – 6050.6	0.017	56	72	0.8	—	—	Eu II, Co I
04	6051.9 – 6058.9	0.111	207	45	4.6	257	13	Cr II, Fe I, S I
05	6060.2 – 6073.6	0.083	93	52	1.8	24	34	Fe I, Cr II, Co I
06	6074.9 – 6084.8	0.074	189	49	3.8	2	15	Fe I, Co I, Fe II
07	6086.2 – 6095.6	0.108	411	45	9.1	208	6	Cr II, Co I, Si I
08	6099.4 – 6109.3	0.183	46	33	1.4	9	45	Ca I, Fe I
09	6110.7 – 6118.1	0.042	405	90	4.5	198	13	Fe II, Si I, Cr II, Co I
10	6120.5 – 6126.9	0.145	49	32	1.5	12	41	Ca I, Si I
11	6127.8 – 6133.8	0.054	71	63	1.1	70	62	Si I, Cr II, Fe I
12	6135.2 – 6139.7	0.134	11	39	0.3	—	—	Fe I
13	6141.0 – 6151.4	0.262	157	31	5.1	274	11	Fe II, Si I, Ba II
14	6153.3 – 6164.6	0.383	178	31	5.7	7	10	Ca I, Si I
15	6166.0 – 6171.5	0.133	60	30	2.0	140	30	Ca I, Fe I
16	6172.9 – 6181.8	0.046	26	65	0.4	—	—	Cr II, Fe II, Eu II
17	6184.1 – 6193.0	0.018	45	42	1.1	321	70	Fe I
18	6194.4 – 6197.5	0.055	507	44	11.5	202	5	Cr II, Si I
19	6198.8 – 6210.2	0.033	195	98	2.0	45	30	Ca II, Cr II, Fe I
20	6212.5 – 6217.5	0.055	140	82	1.7	243	36	Ti II, Fe I
21	6218.4 – 6223.4	0.048	394	86	4.6	352	13	Fe I, Ti II
22	6224.8 – 6228.3	0.016	64	125	0.5	—	—	Cr II, Fe I, V II
23	6229.2 – 6234.7	0.101	26	45	0.6	—	—	Fe I, Co I
24	6236.0 – 6241.5	0.159	105	41	2.6	336	23	Fe II, Si I
25	6242.9 – 6250.3	0.234	84	34	2.5	53	24	Si I, Fe II, Fe I
26	6251.7 – 6263.1	0.138	89	45	2.0	293	31	Fe I, Si I
27	6264.4 – 6274.8	0.045	226	77	2.9	341	20	Co I, Fe I
28	6275.7 – 6287.1	0.478	160	28	5.7	357	10	telluric, Co I
29	6288.9 – 6296.9	0.099	114	39	2.9	36	20	telluric, Fe I
30	6297.7 – 6308.1	0.202	68	29	2.4	308	25	Fe I, telluric
31	6309.0 – 6312.5	0.051	130	51	2.6	334	23	telluric, Si I
32	6313.4 – 6325.3	0.308	130	36	3.6	125	16	Ca I, Fe II, Fe I
33	6326.1 – 6333.6	0.106	460	38	12.2	260	5	Sm II(?), Fe II, Si I
34	6335.0 – 6338.5	0.048	119	56	2.1	17	28	Fe I, Cr II
35	6340.8 – 6350.7	0.319	89	26	3.4	7	17	Si II, Ca I
36	6352.1 – 6367.4	0.266	184	39	4.7	353	12	Ca I
37	6368.3 – 6373.7	0.143	35	29	1.2	287	55	Si II
38	6375.1 – 6387.9	0.090	440	66	6.7	306	9	Fe II, Fe I
39	6389.3 – 6397.2	0.077	100	49	2.0	297	30	Fe I
40	6398.6 – 6402.1	0.066	86	38	2.3	20	26	Fe I
41	6404.5 – 6412.9	0.132	78	30	2.5	14	23	Fe I
42	6414.3 – 6423.2	0.210	245	33	7.4	298	8	Fe II, Fe I, Co I
43	6424.6 – 6435.4	0.152	69	47	1.5	332	43	Fe II, Fe I
44	6436.8 – 6441.3	0.132	86	28	3.1	79	19	Ca I, Eu II
45	6442.2 – 6444.7	0.013	120	95	1.3	100	52	Si I, Fe II, Co I
46	6448.1 – 6452.6	0.146	39	26	1.5	83	42	Ca I, Co I
47	6453.5 – 6460.4	0.363	70	20	3.5	22	17	Fe II, Ca II
48	6461.8 – 6465.3	0.100	93	24	3.9	13	15	Ca I
49	6468.1 – 6478.0	0.218	29	30	1.0	—	—	telluric, Ca I
50	6478.9 – 6488.3	0.152	114	38	3.0	236	19	telluric, Fe II
51	6489.7 – 6501.5	0.422	69	33	2.1	229	28	Ca I, Fe I, Ti II, Ba II

[a] Approximate total equivalent-width of lines in band, relative to local fit across band.
[b] Noise estimated from amplitude spectrum using 1100–2300μHz and 2600–4400μHz.
[c] Phase is calculated with respect to a reference-point (t_0) at JD 2450215.07527, and the convention is that a phase of 0° represents maximum velocity (red-shift).
[d] Error in the phase is taken to be arcsin(rms-noise/amplitude).
[e] Notes on each band giving the probable dominating absorption lines derived from synthetic spectra supplied by Friedrich Kupka (private comm.).

Table 3 – *continued* . Information on wavelength bands from α Cir showing amplitude and phase at 2442.03 μHz from the Stromlo data set. This page of the table shows mainly the bands redward of Hα.

band no.	wavelengths (Å)	total-EW[a] (Å)	amplitude (ms^{-1})	rms-noise[b] (ms^{-1})	signal-to-noise ratio	phase[c] (degrees)	phase-error[d] (degrees)	notes[e] on lines
52	6502.4 – 6509.9	0.012	88	84	1.0	174	73	telluric, Fe I
53	6511.2 – 6521.1	0.395	49	23	2.1	20	29	Fe II, telluric
54	6522.5 – 6529.0	0.110	311	37	8.4	327	7	telluric, Si I
55	6530.3 – 6538.8	0.078	86	60	1.4	6	45	telluric, S I
56	6585.2 – 6589.7	0.055	25	88	0.3	—	—	Fe II, C I
57	6591.1 – 6596.5	0.049	294	67	4.4	207	13	Fe I
58	6597.9 – 6607.3	0.015	989	90	11.0	16	5	Sm II(?), Ti II
59	6608.7 – 6620.0	0.047	156	56	2.8	293	21	Y II, Co I, Fe I
60	6623.9 – 6640.6	0.100	296	69	4.3	64	13	Fe I, Si I, Co I
61	6642.0 – 6652.9	0.066	259	50	5.2	334	11	Eu II
62	6654.2 – 6658.7	0.021	139	189	0.7	—	—	C I, Ca I
63	6660.1 – 6674.9	0.084	199	67	3.0	351	20	Fe I, Cr I, Si I
64	6676.3 – 6682.2	0.100	517	54	9.6	181	6	Fe I, Ti II
65	6683.1 – 6714.1	0.042	267	63	4.3	304	14	Al I, Fe I, Ca I
66	6715.4 – 6719.5	0.062	56	38	1.5	302	43	Ca I
67	6720.8 – 6724.3	0.030	147	69	2.1	213	28	Si I
68	6725.2 – 6746.4	0.040	519	96	5.4	5	11	S I, Fe I
69	6747.3 – 6754.2	0.044	214	107	2.0	324	30	S I, Fe I, Si I
70	6755.6 – 6759.1	0.031	139	78	1.8	272	34	S I
71	6760.5 – 6779.2	0.013	95	112	0.8	—	—	Co I, Si I, Ni I
72	6781.5 – 6788.0	0.030	798	146	5.5	28	11	Ti II
73	6788.9 – 6798.3	0.067	490	80	6.1	33	9	Y II
74	6800.6 – 6823.8	0.021	344	81	4.3	338	14	Co I, Fe I, Si I
75	6826.6 – 6830.1	0.042	171	58	3.0	258	20	Ti II, C I, Fe I
76	6831.5 – 6834.5	0.013	177	149	1.2	59	58	Y II
77	6835.9 – 6850.2	0.153	78	88	0.9	—	—	Fe I
78	6851.6 – 6859.0	0.065	64	56	1.1	138	61	Fe I, Si I
79	6860.4 – 6863.9	0.018	494	114	4.3	1	13	Si I, Fe I, Fe II
80	6864.8 – 6881.0	3.605						telluric reference
81	6881.9 – 6902.1	1.958	36	14	2.5	318	23	telluric
82	6903.0 – 6920.2	0.832	30	10	3.0	263	19	telluric
83	6921.6 – 6966.2	2.424	42	12	3.5	358	16	telluric
84	6968.6 – 7007.4	1.184	45	21	2.2	322	27	telluric
85	6522.0 – 6607.8	10.398	168	13	13.1	325	4	Hα
86	6538.2 – 6590.2	7.774	174	12	14.1	332	4	Hα
87	6545.5 – 6578.4	5.486	166	12	13.7	324	4	Hα
88	6554.3 – 6571.1	2.931	182	12	14.9	328	4	Hα

2σ level, with the exception of bands 58 and 79. These have larger amplitudes when measured using the La Silla data (Table 4). Amplitude variation is not unexpected since the photometric amplitude varies as a function of rotation phase of the star (rotation period 4.48 days, Kurtz et al. 1994). The La Silla time-series may sample the rotational phases of the star in such a way to produce a larger amplitude on average. Other possible reasons are that the bands are not exactly equal for the two data sets (they are slightly out of alignment by about 0.5 to 1 pixel) and that the dispersions are different (see Section 2).

Table 4. Comparison of the large velocity amplitude bands between the Stromlo and the La Silla data sets.

Band no.	Stromlo measurement	La Silla measurement
58	$990\pm 90\,ms^{-1}$	$1660\pm280\,ms^{-1}$
72	$800\pm150\,ms^{-1}$	$960\pm400\,ms^{-1}$
79	$490\pm110\,ms^{-1}$	$1370\pm380\,ms^{-1}$

5 DISCUSSION AND CONCLUSIONS

5.1 Techniques

We have shown that it is possible to obtain high-precision velocity measurements with medium-dispersion spectrographs using telluric lines as a reference. For the Doppler shift of the Hα line, we have obtained a noise level of $500\,ms^{-1}$ per spectrum from Mt. Stromlo and $900\,ms^{-1}$ per spectrum from La Silla. These measurement are not limited by photon-noise, so the difference in precision between the two sites must be due to either the instrument (coudé vs. Cassegrain) or the telluric reference. Given that Mt. Stromlo (750m) is situated at a lower altitude than La Silla (2400m), we note that a possible advantage of low altitude sites is that the telluric

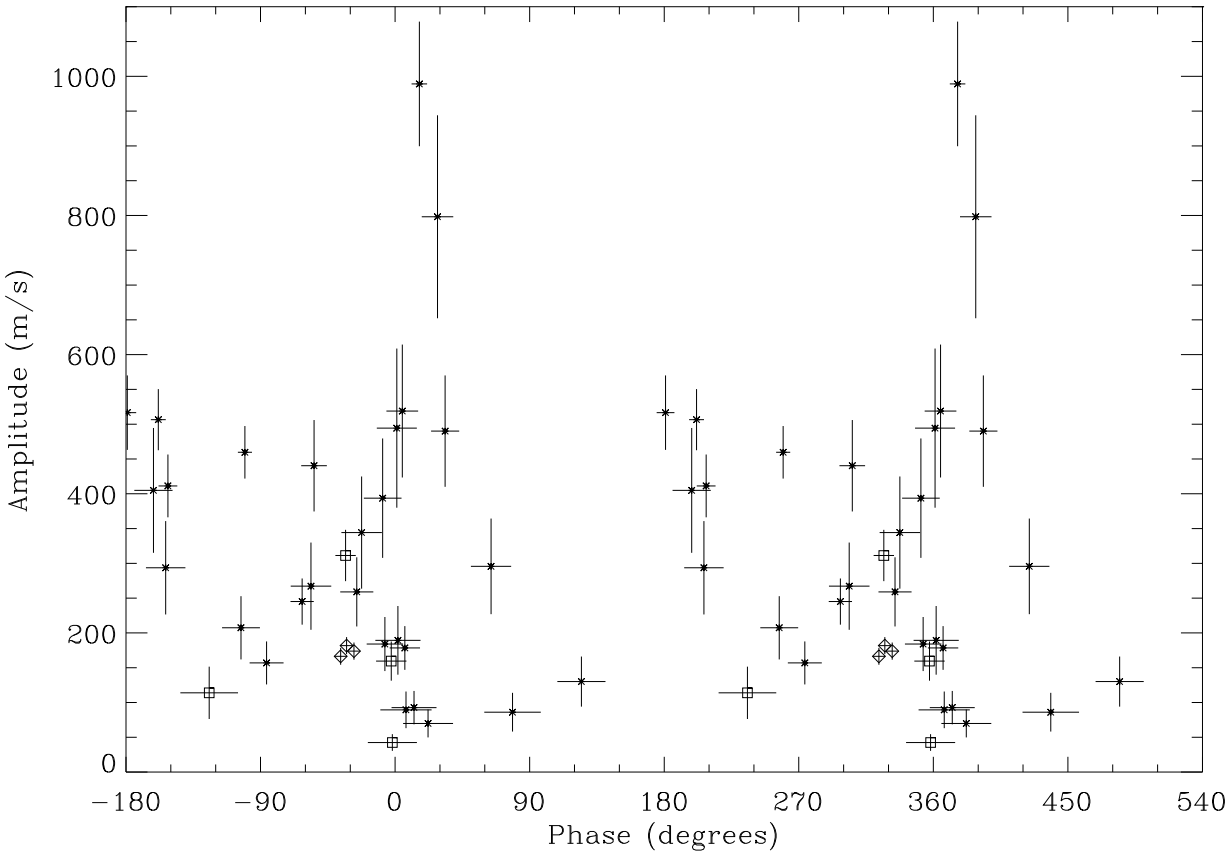

Figure 7. Amplitudes and phases of the principal pulsation mode in α Cir for different wavelength bands, using the Stromlo data. Only the bands with a signal-to-noise ratio greater than 3.0 are plotted. The diamonds represent three different wavelength bands across the Hα line, and the squares represent bands that contain some telluric lines. Note that the data are plotted twice for clarity.

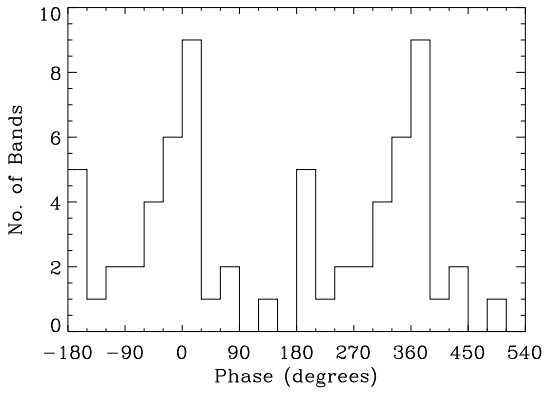

Figure 8. Histogram of the data in Figure 7 in phase bins of 30°. In total, 33 bands are plotted, with only one band across Hα included.

lines are more stable. This is plausible since the lines will be stronger, and temperature and velocity changes will be averaged over a longer distance in the Earth's atmosphere.

We chose the strongest telluric feature (band 80) as our velocity reference. The total equivalent-width (EW) of the metal lines within this band was estimated (using the synthetic spectra) to be approx. 2 percent of the total EW of the band. Other bands (81–84), which are also dominated by telluric lines, show low-amplitude oscillation signals with signal-to-noise ratios from 2.2 to 3.5. This is not surprising since these bands have approx. 6%, 12%, 9% and 23% of their total EW coming from metal lines.

5.2 Velocity Amplitudes

Schneider & Weiss (1989) set an upper limit of 100 ms^{-1} for radial velocity variations in α Cir but this was set assuming no amplitude and phase differences between lines. From their Table 4, it can be seen that only from lines at 6462.6Å and 6494.99Å can amplitudes above 100 ms^{-1} be ruled out. This is in agreement with our measured amplitudes in bands 48 and 51 which are 93±24 ms^{-1} and 69±33 ms^{-1} respectively.

We cannot compare our results directly with the upper limit of only 18 ms^{-1} set by Hatzes & Kürster (1994), but our results show that such a low limit could be set if there were only lines with low amplitude, and perhaps different phases, in the region used by them (5365–5410Å). Kanaan & Hatzes (1997) have measured radial velocity variations in γ Equ in a similar wavelength region (5373–5394Å) and find an average amplitude of 30 ms^{-1}. In conclusion, our mea-

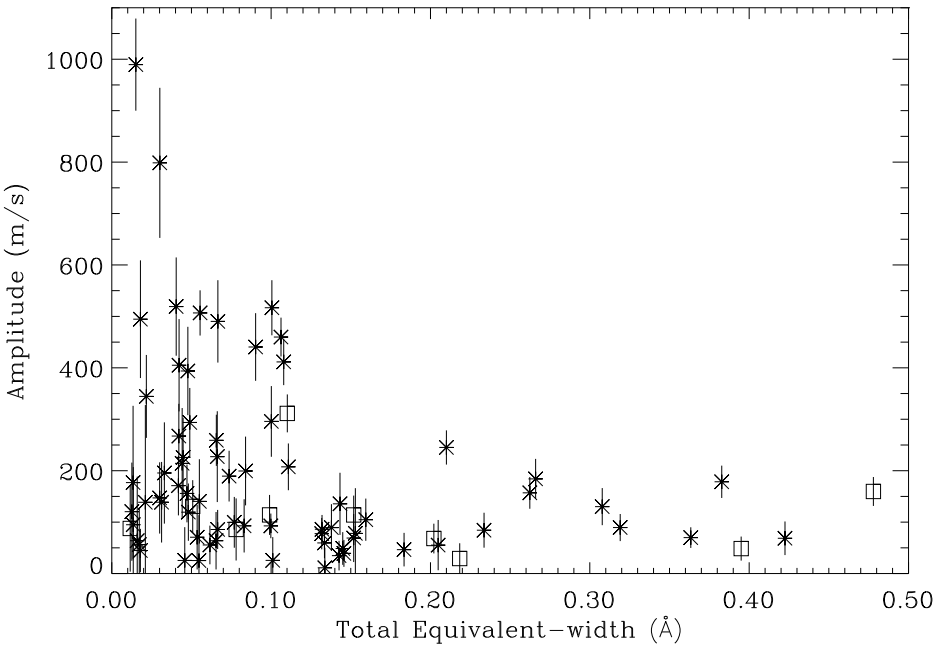

Figure 9. Amplitude of the principal pulsation mode as a function of total equivalent-width for bands 0–79, using the Stromlo data. The squares represent bands that contain some telluric lines.

sured amplitude differences between bands are consistent with previous upper limits on velocity variations in α Cir and are comparable to the amplitude differences found in γ Equ by Kanaan & Hatzes (1997). Furthermore, our data lend support to the detection by Belmonte et al. (1989) of a velocity amplitude of $1000\,\mathrm{ms}^{-1}$ in α Cir.

5.3 Probing the Atmosphere

The photometry of roAp stars has revealed a steep decline of pulsational amplitude with increasing wavelength. Matthews et al. (1990, 1996) have attributed this to the wavelength dependence of limb-darkening. They have determined limb-darkening coefficients from their amplitude measurements of HR 3831. However, Medupe & Kurtz (1997, see also Medupe 1997) suggest that limb-darkening is too small an effect to explain the observed decline. Instead, they account for the decline by the change in pulsational temperature amplitude with depth in the stars, α Cir and HR 3831. This result would imply a surprisingly small radial node separation in the atmosphere of roAp stars (Matthews 1997). The amplitude and phase variations presented in this paper (see also Viskum et al. 1997) suggest the same, with a radial-node situated in the atmosphere of α Cir. Matthews (1997) suggested an alternative interpretation, where ions are grouped either side of a horizontal node on the surface. Since we can find no simple pattern associating ion type with amplitude or phase, we argue that the phase differences are probably caused by differing formation depths and therefore there is a radial-node in the atmosphere.

Three bands (Table 4) have a particularly large amplitude in one or both data sets. It could be these bands contain elements that are located in spots on the surface of the star, near a pole of the dipole pulsation, which is why their velocity amplitude is larger. The argument against this hypothesis is that there is no one element that is a dominating factor in all three bands. However, we can not rule out surface inhomogeneities as a factor contributing to the amplitude and phase variations.

5.4 Further Work

A time-series of high-resolution spectra would be invaluable in explaining the complete range of amplitudes and phases discovered in α Cir. With our results, we can not rule out significant contributions from blending effects to the amplitudes and phases of different bands. However, with our data set from 1996 May we can look for Hα line profile variations. In particular, measuring the width and velocity amplitude at different depths in the Hα line (Baldry et al., Paper II).

Eventually, spectroscopy of α Cir combined with modeling, should be able to map the shape of the pulsation wave in the atmosphere of the star.

6 ACKNOWLEDGEMENTS

Many thanks to Don Kurtz, Jaymie Matthews, Jørgen Christensen-Dalsgard and others, with whom we had fruitful discussions at IAU Symposium 181 in Nice. Thanks (again) to Don Kurtz for providing photometric data, and to Friedrich Kupka for providing synthetic spectra. Also we are grateful to Michael Bessell for his help and advice in setting up the instrument at Mt. Stromlo, and to the Director of Mt. Stromlo Observatory and the Danish time allocation

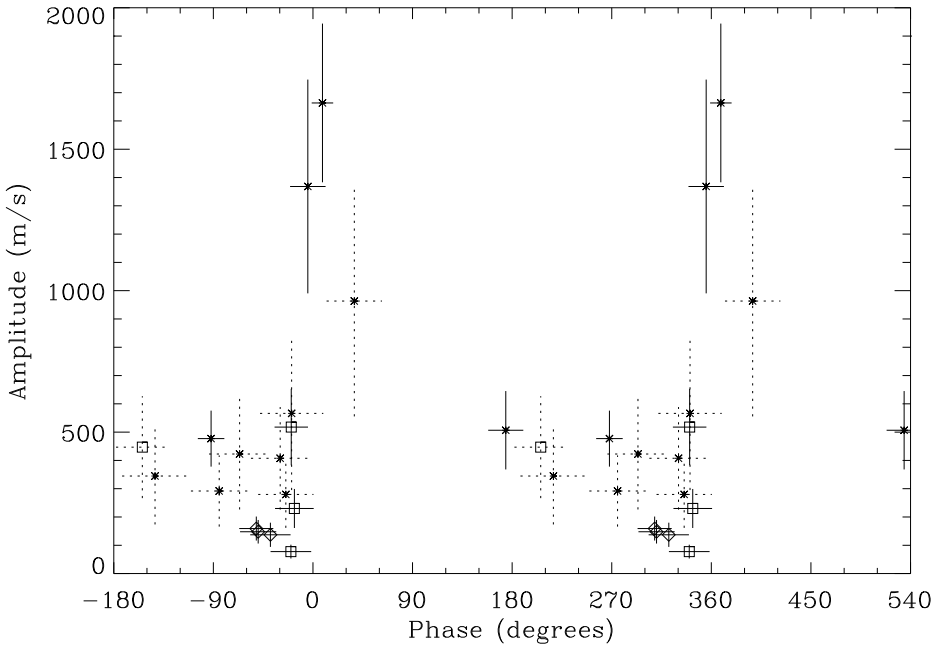

Figure 10. Amplitudes and phases of the principal pulsation mode for different bands using the La Silla data (which covers bands 23–88). This figure is similar to Figure 7 except: additionally the bands with a signal-to-noise ratio between 2.0 and 3.0 are plotted, with dotted lines. Also note that the amplitude scale extends to $2000\,\mathrm{ms}^{-1}$ rather than $1100\,\mathrm{ms}^{-1}$.

committee for the telescope time. We acknowledge the Harvard ADS Abstract Service as an invaluable aid in finding relevant papers.

This work was carried out while Ivan Baldry was in receipt of an Australian Postgraduate Award, and was also supported by funds from the Australian Research Council and the Danish Natural Science Research Council through its Center for Ground-based Observational Astronomy. This work was supported in part by the Danish National Research Foundation through its establishment of the Theoretical Astrophysics Center.

REFERENCES

Baldry I.K., Viskum M., Bedding T.R., Kjeldsen H., Frandsen S., in prep. (Paper II)
Belmonte J.A., Bell C.R., Leeper M., Pallé P.L., Pietraszewski K.A.R.B., Renton R.E., Cortés T.R., 1989, A&A, 221, 41
Gilliland R.L. et al., 1993, AJ, 106, 2441
Hatzes A.P., Kürster M., 1994, A&A, 285, 454
Kanaan A., Hatzes A.P., 1997, ApJ, in press
Kjeldsen H., Bedding T.R., 1995, A&A, 293, 87
Kurtz D.W., 1990, ARA&A, 28, 607
Kurtz D.W., Martinez P., 1993, in Dworetsky M.M., Castelli F., Faraggiana R., eds, ASP Conf. Ser. Vol. 44, Peculiar Versus Normal Phenomena in A-Type and Related Stars. Astron. Soc. Pacific, San Francisco, p. 561
Kurtz D.W., Sullivan D.J., Martinez P., Tripe P., 1994, MNRAS, 270, 674
Kurtz D.W., van Wyk F., Roberts G., Marang F., Handler G., Medupe R., Kilkenny D., 1997, MNRAS, 287, 69
Kupka F., Ryabchikova T.A., Weiss W.W., Kuschnig R., Rogl J., Mathys G., 1996, A&A, 308, 886
Libbrecht K.G., 1988, ApJ, 330, L51
Martinez P., Kurtz D.W., 1995a, Ap&SS, 230, 29
Martinez P., Kurtz D.W., 1995b, in Stobie R.S., Whitelock P.A., eds, ASP Conf. Ser. Vol. 83, Astrophysical Applications of Stellar Pulsation. Astron. Soc. Pacific, San Francisco, p. 58
Mathys G., Kharchenko N., Hubrig S., 1996, A&A, 311, 901
Matthews J.M., 1991, PASP, 103, 5
Matthews J.M., 1997, in Provost J., Schmider F.X., eds, Proc. IAU Symp. 181, Sounding Solar and Stellar Interiors. Kluwer, Dordrecht, in press
Matthews J.M., Chagnon F., 1997, in Bradley P.A., Guzik J.A., eds, ASP Conf. Ser., A Half Century of Stellar Pulsation Interpretations. Astron. Soc. Pacific, San Francisco, in press
Matthews J.M., Wehlau W.H., Walker G.A.H., Yang S., 1988, ApJ, 324, 1099
Matthews J.M., Wehlau W.H., Walker G.A.H., 1990, ApJ, 365, L81
Matthews J.M., Wehlau W.H., Rice J., Walker G.A.H., 1996, ApJ, 459, 278
Medupe R., 1997, in Schmider F.X., Provost J., eds, Poster Proc. IAU Symp. 181, Sounding Solar and Stellar Interiors. Univ. Nice, in press
Medupe R., Kurtz D.W., 1997, MNRAS, submitted
Perryman M.A.C. et al., 1997, A&A, 323, L49
Rice J.B., Wehlau W.H., 1991, A&A, 246, 195
Schneider H., Weiss W.W., 1989, A&A, 210, 147
Shibahashi H., 1991, in Gough D., Toomre J., eds, Lecture Notes in Physics 388, Challenges to Theories of the Structure of Moderate-Mass Stars. Springer-Verlag, Berlin, p. 393
Viskum M., Baldry I.K., Kjeldsen H., Frandsen S., Bedding T.R., 1997, in Schmider F.X., Provost J., eds, Poster Proc. IAU Symp. 181, Sounding Solar and Stellar Interiors. Univ. Nice, in press
Weiss W.W., Schneider H., Kuschnig R., Bouchet P., 1991, A&A, 245, 145